Vortex flow patterns near critical state for onset of convection in air flow through a bottom heated horizontal flat duct

J.T. Lir, M.Y. Chang, Tsing-Fa Lin*

Department of Mechanical Engineering, National Chiao Tung University, 1001 Ra Hsueh Road, Hsinchu 30049, Taiwan

Abstract

In this paper, an experiment is carried out to investigate the buoyancy driven vortex flow at slightly subcritical and supercritical Rayleigh numbers in a mixed convective air flow through a bottom heated horizontal flat duct. Particular attention is paid to the flow at a very low Reynolds number for $3.0 \leq Re \leq 5.0$. Results from the flow visualization have revealed two new vortex flow patterns in addition to those often seen in literature such as longitudinal rolls (L rolls), moving transverse rolls (T rolls), and mixed longitudinal/transverse rolls (M rolls). The newly observed vortex flow patterns include the stable longitudinal rolls near the duct sides along with nonperiodic traversing transverse waves in the duct core, and the mixed longitudinal and transverse rolls as well as irregular cells. Moreover, steady longitudinal rolls and nonperiodic traversing transverse waves are noted even at subcritical Rayleigh numbers. A flow regime map delineating various vortex flow patterns is given. Temporal characteristics of the flow are also inspected. Furthermore, a correlation is given to estimate the local onset locations of the longitudinal rolls. Meanwhile, the oscillation frequency and convection speeds of the transverse rolls are correlated from the present data. Finally, many complicate processes during the vortex flow formation are noted, such as the generation of the L and T rolls and transverse waves, splitting of rolls into cells and the reverse process of cell integration into rolls, aside from the moving and bending of T rolls. © 2001 Elsevier Science Ltd. All rights reserved.

Keywords: Vortex flow; Near critical mixed convection; Flat duct

1. Introduction

Considerable research has been carried out recently to study the buoyancy driven vortex flow in mixed convection of gas through a horizontal flat duct due to its importance in various technological processes such as cooling of microelectronic equipments [1], design of compact heat exchangers [2] and thin crystal film growth from chemical vapor deposition (CVD) [3–5]. At moderately supercritical Rayleigh numbers various vortex flow structures such as longitudinal rolls, transverse rolls and mixed longitudinal/transverse rolls have been reported in the literature. However, in the limiting Rayleigh number very close to the onset of convec-

* Corresponding author. Tel.: +886-35712121-55118; fax: +886-35726440.
E-mail address: u8614812@cc.nctu.edu.tw (T.-F. Lin).

Nomenclature

A	aspect ratio, b/d	t_p	oscillation period (s)
b, d	channel width and height	T	temperature
f, F	dimensional and dimensionless frequencies, $F = f/(\alpha/d^2)$	T_c, T_h	temperatures of cold and hot plates
g	gravitational acceleration	T_m	mean temperature, $(T_h + T_c)/2$
Gr	Grashof number, $\beta g d^3(T_h - T_c)/v^2$	W, W_m	velocity and average velocity components in z direction
Pr	Prandtl number, v/α	W_r	wave speed of the transverse rolls
Ra	Rayleigh number, $\beta g d^3(T_h - T_c)/\alpha v$	x, y, z	dimensionless cartesian coordinates scaled with d
Ra_c	critical Rayleigh number corresponding to onset of convection	α	thermal diffusivity
Ra_z	local Rayleigh number, $\beta g z^3(T_h - T_c)/\alpha v$	β	thermal expansion coefficient
Re	Reynolds number, $\frac{W_m \times d}{v}$	θ	dimensionless temperature, $\frac{(T-T_m)}{(T_h-T_c)}$
t	time (s)	v	kinematic viscosity

---

tion for $Ra \approx 1708$, the vortex flow can be very different from those at high Ra and remains largely unexplored. Some unusual vortex flow patterns may appear, as discussed by Koschmieder [6] on natural convection in a shallow cavity.

The critical Rayleigh number Ra_c^L for the onset of longitudinal vortex rolls in a mixed convective flow through a bottom heated horizontal flat duct was found to be 1708 [7–12]. It is well known that Ra_c^L is unaffected by the Reynolds number Re. But the critical Rayleigh number for the onset of the transverse rolls Ra_c^T increases with the Reynolds number Re [13,14]. Slightly above the critical Rayleigh number Ra_c^L, steady longitudinal rolls prevail for $Re \geq 9$ and the roll diameter is nearly equal to the duct height [8]. As the Rayleigh number is well above Ra_c^L, there is no stable vortex rolls [9,10].

Flow regime maps in terms of the Reynolds number versus Rayleigh number were proposed by various workers to delineate the flow with no vortex roll, steady and unsteady longitudinal, transverse and intermittent rolls [15–19]. Kamotani et al. [12] indicated that in the thermal entrance region the heat transfer rate was affected not only by the Rayleigh number but also by the buoyancy-to-inertia ratio Gr/Re^2.

Luijkx and Platten [13] proved the existence of the transverse thermoconvective rolls in mixed convection of silicone oil ($Pr \approx 450$) through a bottom heated horizontal plane channel at a very low Reynolds number, $0.001 \leq Ra \leq 0.01$. The critical Rayleigh number for the onset of the transverse rolls Ra_c^T was found to be a function of the aspect ratio and Prandtl number. Ouazzani et al. [17–19] refined the flow regime maps to include the transverse rolls for air flow with $1 < Re < 9$ and $12,000 \leq Ra \leq 20,000$. They also found a particular

flow regime that appeared approximately between $1920 < Ra < 2082$ and $0.45 < Re < 0.75$, in which only irregular and intermittent flow structure was observed. Recently, Chang and Lin and their colleagues [20–24] carried out detailed flow visualization and temperature measurement to explore the mixed convective air flow for $Re \leq 50$ and $30,000 \geq Ra \geq 1800$. They revealed six vortex flow patterns: (1) stable longitudinal rolls, (2) unstable longitudinal rolls, (3) unstable longitudinal to transverse roll transition, (4) mixed longitudinal/transverse rolls, (5) transverse rolls and (6) irregular rolls.

In an experimental study Kamotani et al. [12] indicated that the steady longitudinal vortex flow became unstable once the fully developed vortex rolls occupied the entire test section in a long plane channel. For a larger duct aspect ratio the flow is more irregular. Moffat and Jensen [25,26] suggested that the bouyancy driven secondary flow structure was very sensitive to the aspect ratio of the duct.

Similar investigations with the bottom plate heated by a uniform heat flux were conducted by Incropera et al. [27–30]. Four flow regimes with progressing complexity were identified along the channel, beginning with laminar forced convection near the duct inlet, followed by laminar mixed convection, transitional mixed convection and turbulent free convection.

The above literature review clearly indicates that the buoyancy driven vortex flow in a mixed convective gas flow through a flat duct at a low Rayleigh number just exceeding the critical level remains largely unexplored. In the present study, an experiment combining the flow visualization and temperature measurement is carried out to investigate the temporal and spatial characteristics of the vortex flow structure induced in mixed
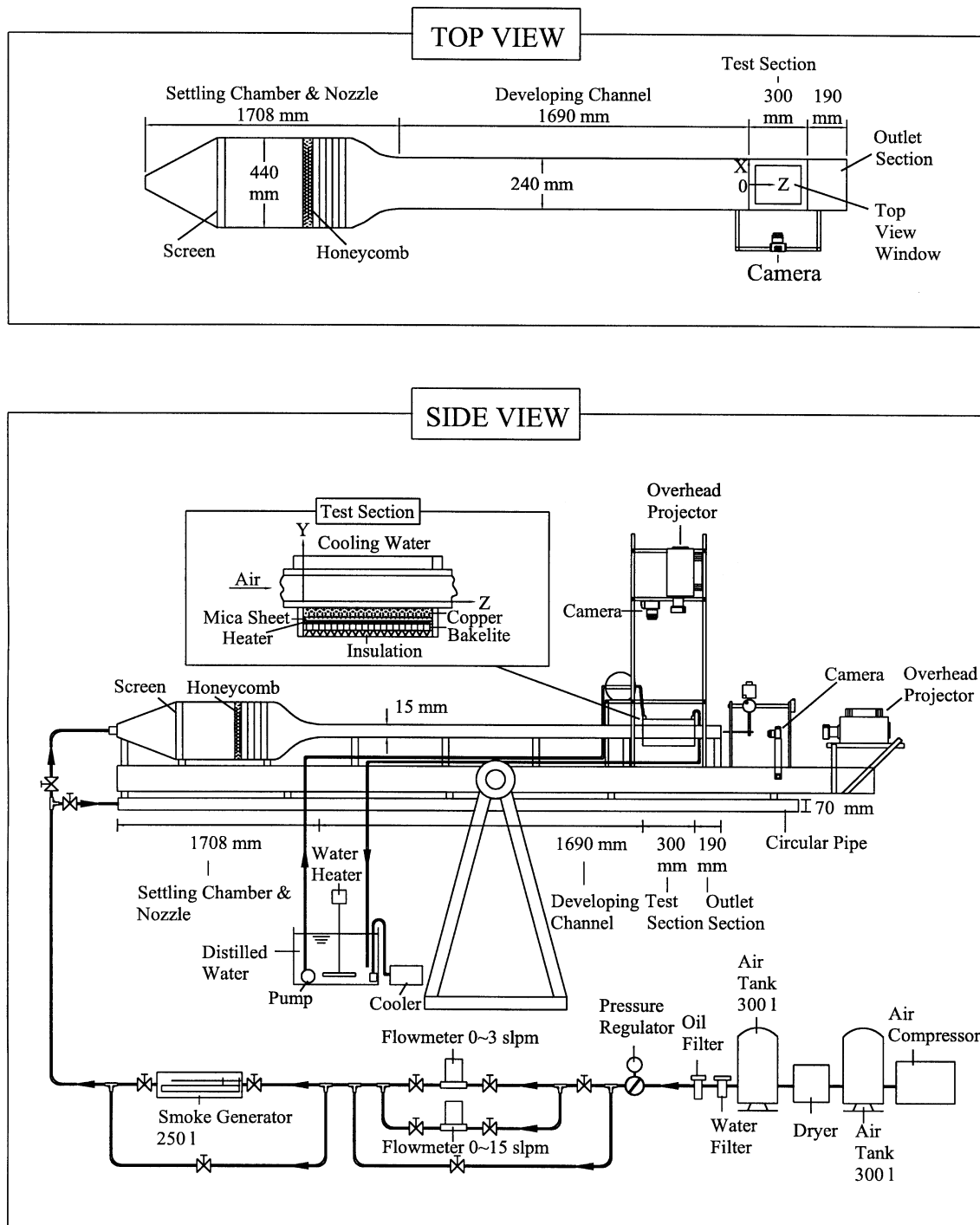
Fig. 1. Schematic of test apparatus and the chosen coordinate system.

convection of air through a bottom heated, horizontal flat duct at very low Reynolds number with Re varying from 3 to 5. This low Reynolds number flow is typical for CVD processes [5]. Note that at this low Reynolds number the bouyancy-to-inertia ratio Gr/Re^2 is still relatively high even for the slightly subcritical Rayleigh number and it is reasonable to expect the existance of some vortex flow at the subcritical state [6]. Thus, the Rayleigh number will be varied from 1200 to 4000.

2. Experimental apparatus and procedures

2.1. Experimental apparatus

The schematic diagram of the test apparatus which is modified slightly from our previous study [20,23,24] is shown in Fig. 1. The open-loop mixed convection apparatus consists of three parts: wind tunnel, test section, and measuring bench for the velocity and temperature probes along with the data acquisition system. The test section is a rectangular duct 240 mm wide and 300 mm long with 15 mm in height between the top cooled and bottom heated plates, providing an aspect ratio of $A = 16$. It should be noted that the duct height is reduced from 20 mm used in our previous study to 15 mm in this study. This narrower gap ($d = 15$ mm) could provide a better control of the temperature difference between the horizontal plates even at very low Rayleigh numbers to be covered in the present study, since at the same low Rayleigh number the temperature difference ΔT is much larger for $d = 15$ mm in view of the fact that $Ra \propto d^3 \cdot \Delta T$. Thus the experimental uncertainty in maintaining a constant ΔT exhibits much smaller effect on the measured data. The bottom plate of the test section is made of a 20 mm thickness, high purity copper plate and is heated by DC power supplies. In order to insure uniform bottom plate temperature, the heaters attached onto the outside surface of the bottom copper plate are divided into 10 segments in the main flow direction and each heater is independently controlled by a GW GPC 3030 D laboratory power supply. In order to reduce the edge effect of the test section, the width of the bottom copper plate is 40 mm larger than the bottom of test section. The top plate of the test section is made of 3 mm thick glass plate and 2 mm thick plexiglass plate with a gap width of 3 mm. This top plate is reinforced by copper alloy frames to keep it flat. Distilled water is provided from a tank and flows into this gap to cool the upper plate. The distilled water is maintained at a constant temperature by a constant temperature circulation unit that consists of a cooler, a heater and a 200 l distilled water reservoir. This cooling unit can control the temperature of the distilled water within ± 0.1°C. The water flow rate is adjusted carefully to keep the

temperature difference over the top plate within ± 0.1°C. The water head is also suitably adjusted to minimize any possible deformation in the glass plate.

The working fluid is air which is driven by a 7.5 hp air compressor and is sent into a 300 l and 100 psi high-pressure air tank. The air is first regulated by a pressure regulator and then is passed through a settling chamber, a contraction nozzle, a developing section and finally the test section. The purpose of forcing the air through the settling chamber is to reduce the air turbulence by installing a diffuser buffer section, two fine mesh screens, a honeycomb section and finally four fine mesh screens in the settling chamber. The air turbulence and flow separation are further suppressed by the contraction nozzle section with a contraction ratio of 20:1, which provides a nearly uniform velocity at the inlet of the developing section.

The developing section is 1660 mm in length, approximately 110 times of the duct height. This insures the flow being fully developed at the inlet of the test section for $Re \leq 50$. An insulated outlet section of 160 mm length is added to the test section to reduce the effects of the disturbances from discharging the flow to the ambient surrounding of the open-loop wind tunnel. The developing and outlet sections are both made of 5 mm thick plexiglass plates, whereas the settling chamber and contraction nozzle are made of stainless steel plates. The entire loop is thermally insulated with a superlon insulator of 20 mm thickness and is bounded on a rigid supporting frame.

The volume flow rate of air is controlled and measured by two Hasting HFC flow controllers designed especially for low volume flow rates, with accuracy better than 1%. In particular, the low air flow rate is controlled precisely by the thermal mass flow sensing technique [31]. These two flow controllers individually operate in the ranges of 0–15 and 0–3 l/min, and they are calibrated by a Brooks bell prover with an accuracy of 0.2%. The operating condition of the flowmeter in the actual experiment is adjusted to a condition similar to that of the calibration stand.

The temperature of the test section is monitored by 13 calibrated and electrically insulated copper–constantan (T-type) thermocouples embedded in the bottom plate and six T-type thermocouples stuck to the inside surface of the top plate. The temperature of both plates could be maintained at nearly uniform and constant values with the deviations ranging from ± 0.05 to ± 0.12°C. Additional thermocouples are used to measure the temperature of the inlet and outlet air. For each experiment, the top plate temperature is kept at the same values as that of the inlet air flow for the purpose of eliminating the formation of a thermal boundary layer on the top wall. The thermcouple signals are recorded by the Computer Products RTP 743 data acquisition system with a resolution of ± 0.05°C.

A thermocouple probe, which is an Omega (model HYP-O) mini hypodermic extremely small T-type thermocouple (33 gauge) implanted in a 1 in. long stainless steel hypodermic needle, is used to measure the instantaneous temperature of the air flow in the duct. The probe is supported by a three-way traversing stand, which is inserted into the flow from the exit end of the channel. In addition, the velocity profile is measured by a hot-wire probe. For calibrating the hot wire, the pipe flow method that the probe is placed in the center of a fully developed laminar pipe flow is used. The total volume flow rate is measured and the pipe center velocity is calculated from the parabolic distribution. These data are recorded by an HP data acquisition system (Hewlett-Packard VXI series-E1411B multimeter and E-1347A multiplexers).

2.2. Analysis of temperature oscillation

In order to unravel the unsteady characteristics of the vortex flow, the transient temperature oscillations are obtained at selected detection points. The sampling rate of the data channel in the data acquisition system is set at 0.08 s per scan which is much shorter than the period of the flow oscillation in the low Reynolds number mixed convective flow considered here.

2.3. Preliminary investigation of flow field and experimental procedures

In order to confirm the fully developed laminar flow at the entrance of the test section, the main forced flow distribution is measured by a hot wire probe which is operated by a constant temperature anemometer (DANTEC Probe Type 55P01 with 56C17 CTA Bridge). The measured data indicated that at the inlet of the test section the velocity profile is fully developed and is in good agreement with the analytical results given by Shah and London [32]. Besides, the turbulence intensities in the flow were found to be less than 1%, implying that the effects of the free stream turbulence on the mixed convective flow characteristics were moderate.

Flow visualization is performed by injecting smoke tracer into the flow to observe the secondary flow structure. Specifically, the tiny incense smoke is injected into the main flow at some distance ahead of the settling chamber. By using a 1.5–2.5 mm plane light beam of an overhead projector with an adjustable knife edge to illuminate the flow field containing these smoke particles, a sharp contrast could be obtained between the duct walls and the smoke.

For each case in the experiment we first impose a fully developed flow in the entire test section and then turn on the DC power supplies to raise the bottom plate temperature. Meanwhile, the distilled water is circulated over the top plate. Each case takes about 3 h to raise the Rayleigh number to the test point and another 2 h are needed to maintain the vortex flow at the stable or statistical state. After this we start various measurements and flow visualization. For the transient tests to observe the vortex flow formation the Reynolds number is changed to the test points in about 10–20 s.

2.4. Analysis of data uncertainty

In order to reduce any possible bias and data reduction errors between the true physical value and the readout of the sensors and transducers, the data acquisition systems and various instruments including multiplexers (Computer Products RTP 743), a digital barometer (Drunk Products DPI-260), reference junctions (Celesco Transducer Products BRJ14), and Hasting mass flow controllers (HFC-220E and HFC-220F) are calibrated and adjusted end to end on site by the Instrument Calibration Section, Q.A. Center, Chung Shan Institute of Science and Technology (CSICI), Taiwan, with the transfer standards that the calibration hierarchy can trace back to the standard of National Institute of Standard and Technology (NIST), USA. Before performing the end to end calibration all the sensors and transducers used were transported to CSIST for calibration or adjustment with the inter-lab standards based on the test point that will be encountered in the present test to get best calibration curve-fit data. The data reduction error is reduced further by using the best nonlinear least square calibration curve-fits and by selecting a suitable gain code of the multiplexers.

Uncertainties in the Rayleigh number, Reynolds number and other independent parameters are calculated according to the standard procedures established by Kline and McClintock [33]. The uncertainties of the thermophysical properties of the air are included in the analysis. The fluid properties are real time corrected based on the temperature and pressure detected at the inlet of the test section. In addition, the uncertainties of the control unsteadiness and temperature nonuniformity are accounted for in the evaluation of the data uncertainty. The analysis shows that the uncertainties of temperature, volume flow rate, dimensions, Reynolds number and Rayleigh number measurements are estimated to be less than $\pm 0.05°C$, $\pm 1\%$, ± 0.05 mm, $\pm 2\%$ and $\pm 5\%$, respectively.

3. Results and discussion

Various vortex flow structures observed in the present study are summarized by a flow regime map shown in Fig. 2. It is important to note from these

results that at this low Reynolds number, $3 \leq Re \leq 5$, the buoyancy driven vortex flow is not completely dominated by the moving transverse rolls, as observed in the previous studies [17–20]. In fact, at slightly supercritical Rayleigh number mixed longitudinal/transverse vortex flow appears. This mixed vortex flow may contain irregular cells in the downstream for $Re = 3$ at $Ra = 2000$. In addition, near and below the critical Rayleigh number we even have longitudinal vortex flow in the duct. It is further noted that for cases near Ra_c transverse waves appear nonperiodically in time in the duct core. Selected results from the present study will be examined in the following sections to illustrate the detailed characteristics of the above vortex flow patterns.

3.1. Vortex flow patterns near critical Rayleigh number

To clearly illustrate the vortex flow patterns induced at the low Rayleigh number around the critical level for the onset of convection ($Ra_c = 1708$), top view of the flow at the midheight of the duct ($y = 0.5$) for various Re and Ra is shown in the following. For cases in which the flow evolves to steady state the steady top view flow photos are given. While for the other cases the flow does not reach steady state at long time, the instantaneous photos at certain time instants in the statistical state are given. Firstly, the change in the vortex flow patterns for Ra reduced from 4000 to 1200 at $Re = 5.0$ is displayed in Fig. 3. The results indicate that for the highest Rayleigh number tested here, with $Ra = 4000$, the vortex flow in the entire duct is dominated by the downstream moving transverse rolls (Fig. 3(a)). The transverse rolls are generated periodically in time in the entry region of the duct and move gradually downstream. The time period of this roll generation is 4.35 s. As the rolls leave the heated section, they gradually degenerate and finally disappear. It is noted that in the ranges of Re and Ra covered here the boundary between the pure transverse vortex flow and the mixed longitudinal/transverse vortex flow indicated in Fig. 2 can be roughly characterized by the
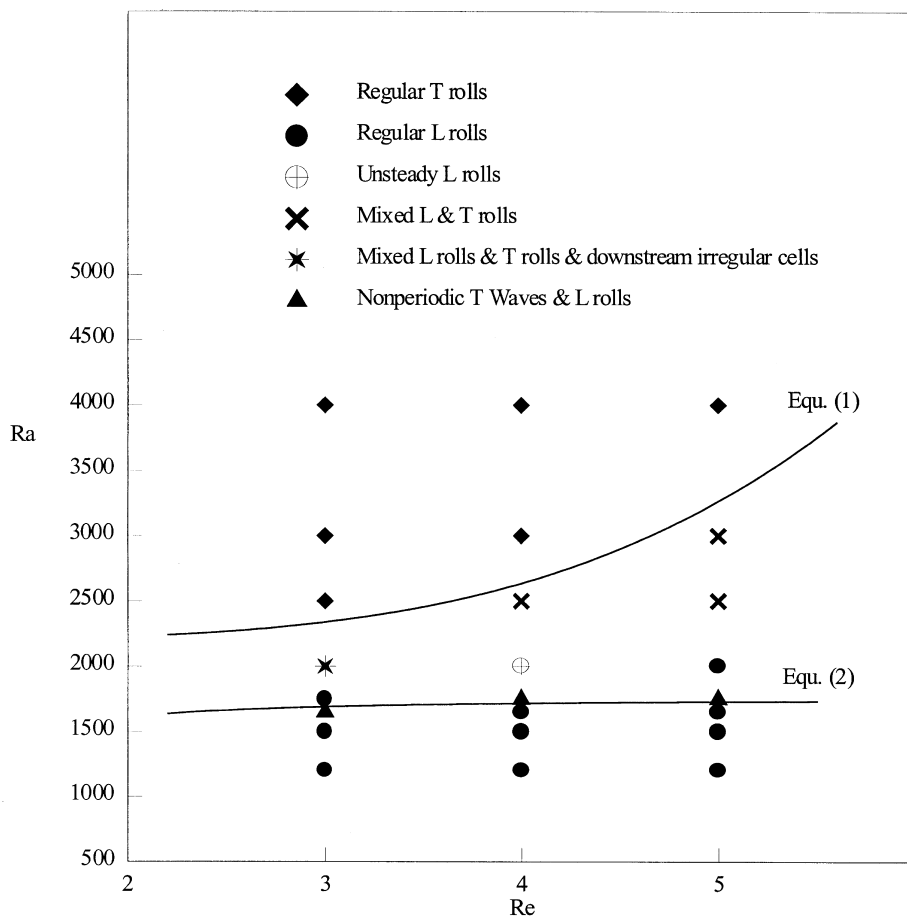

Fig. 2. Flow regime map for different types of flow pattern observed by flow visualization.

equation

$$Ra = 2200 + 1.7Re^4 \qquad (1)$$

At the lower buoyancy, with $Ra = 3000$, the time periodic moving transverse rolls are weaker and only dominate in the duct core (Fig. 3(b)). Near each duct side two steady longitudinal vortex rolls prevail. Thus, we

have mixed longitudinal/transverse vortex flow at $Ra = 3000$. Note that the slow axial growth of the longitudinal rolls in the downstream direction squeezes the transverse rolls and causes them to bend slightly and to become shorter as they move downstream. Moreover, at the juncture between the transverse and longitudinal rolls the vortex flow is somewhat irregular. As the buoyancy is reduced further to $Ra = 2500$, the
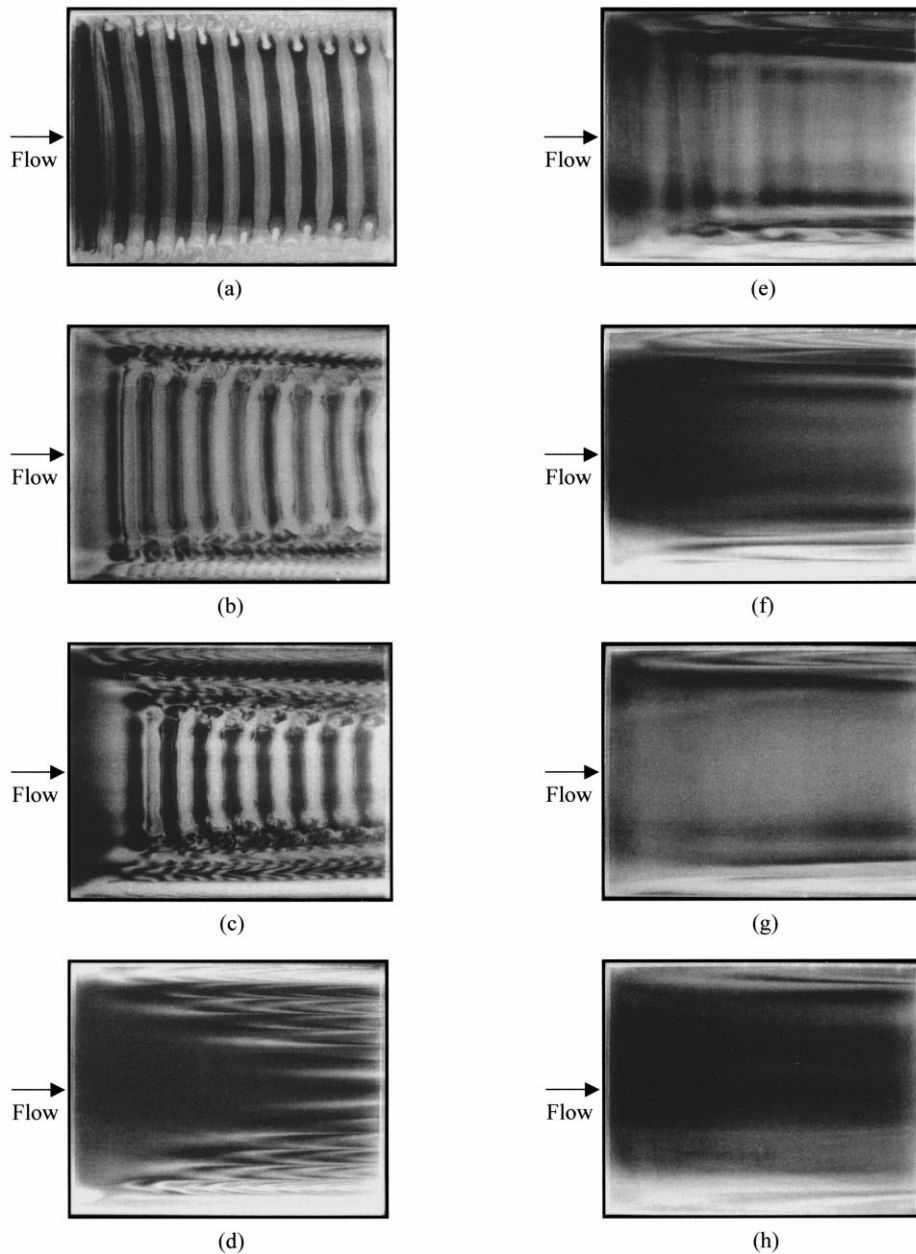

Fig. 3. Top view flow photos at steady or statistical state for $Re = 5.0$ and Ra (a) 4000, (b) 3000, (c) 2500, (d) 2000, (e) 1750, (f) 1650, (g) 1500 and (h) 1200.

transverse rolls weaken further and occupy a smaller region and more longitudinal rolls are induced near the duct sides (Fig. 3(c)). Note that for an even lower buoyancy with $Ra = 2000$ the transverse rolls completely disappear and steady longitudinal rolls dominate the entire vortex flow at long time (Fig. 3(d)). It is of interest to observe that for a reduction of Ra to a slightly supercritical level of 1750 only two steady longitudinal rolls are induced near each duct side and in the duct core a number of downstream moving, weak transverse waves prevail (Fig. 3(e)). These traversing waves are generated nonperiodically in time in the duct entry. Note that the nonperiodic traversing transverse waves appear in a very narrow range of the Rayleigh number around the curve fitted from the present data in Fig. 2 as

$$Ra = 1750 - 540/Re^2 \qquad (2)$$

As the buoyancy is lowered even further to the subcritical level with $Ra = 1650$, 1500 and 1200 these waves disappear but a few longitudinal rolls are still induced in the side wall region (Fig. 3(f)–(h)). The appearance of the longitudinal rolls at the subcritical buoyancy is

further verified by the end view flow photos shown in Fig. 4. According to Fig. 3(d) the axial location at which each longitudinal roll begins to appear depends on its spanwise position. Based on the present data for all cases with steady longitudinal vortex flow, this onset location can be correlated as

$$\ln Ra_z = 11.88 - 0.0367(x)^2 + 0.471 Re_z^{0.5} \qquad (3)$$

Another new vortex flow pattern containing longitudinal and transverse rolls and irregular cells is revealed in Fig. 5 by showing the top view flow photos for various Reynolds numbers at $Ra = 2000$. These photos manifest that at $Re = 5.0$ steady longitudinal rolls dominate in the flow (Fig. 5(a)), as already discussed above. For the lower Re of 4.0 the buoyancy-to-inertia ratio is higher and the longitudinal rolls become unsteady (Fig. 5(b)). A further lowering of Re to 3.0 causes a few transverse rolls to appear in the entry portion of the duct (Fig. 5(c)). Besides, the longitudinal rolls in the duct core downstream of the transverse rolls become unstable and disintegrate into a number of irregular cells. Thus, at $Re = 3.0$ the new vortex flow is in the form of steady longitudinal rolls near the
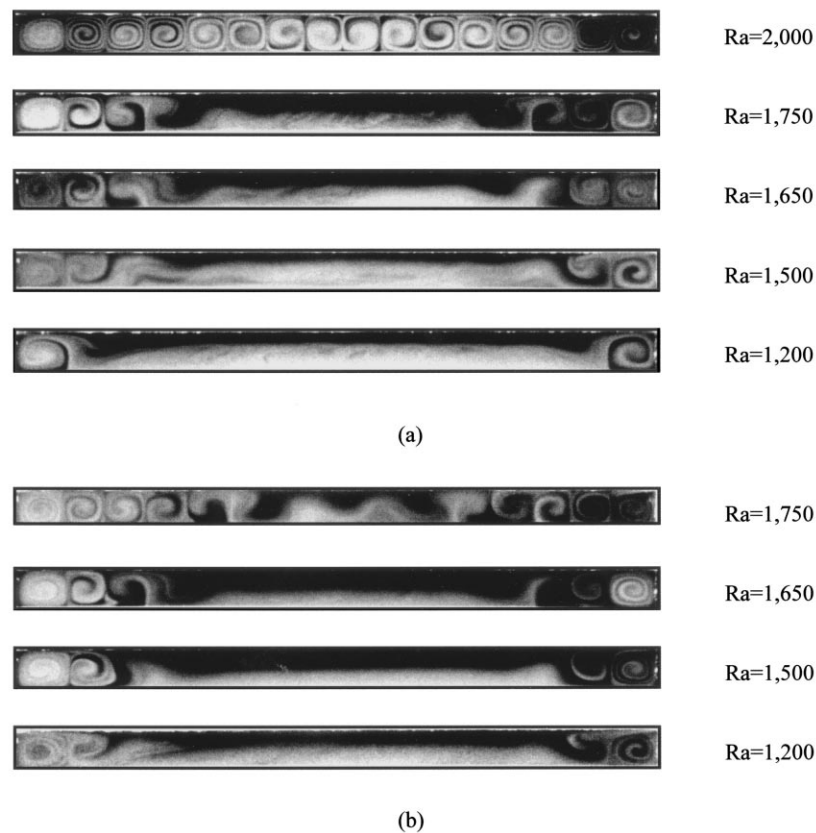

(a)

(b)

Fig. 4. End view of vortex flow at steady or statistical state for various Rayleigh numbers at $z = 19.07$ for Re (a) 5.0 and (b) 3.0.

duct sides, time periodic moving transverse rolls in the duct entry and irregular cells in the remaining region of the duct. Note that the irregular cells are prevalent in a larger region for a higher buoyancy-to-inertia ratio.

3.2. Temporal characteristics of vortex flows

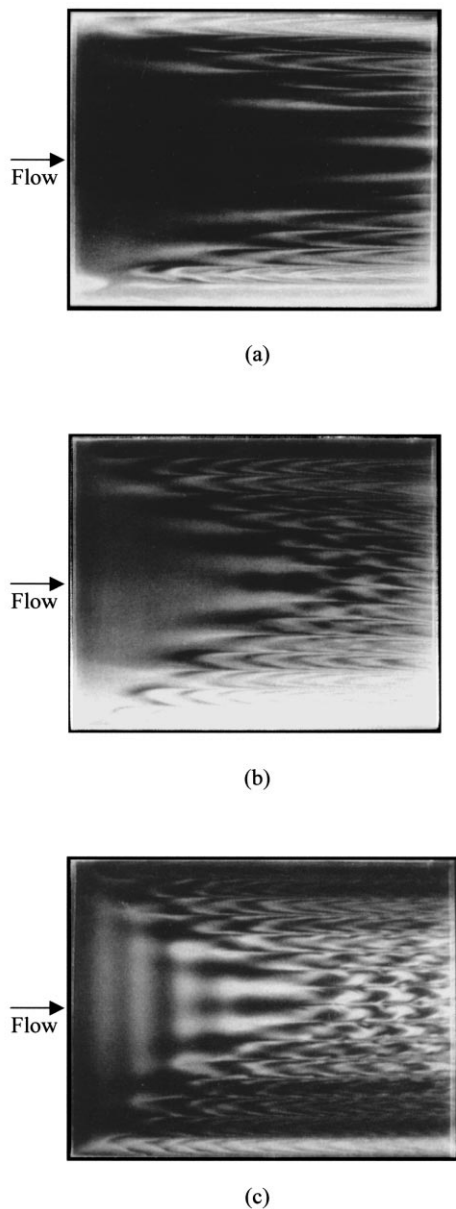The temporal characteristics of the observed vortex

(a)

(b)

(c)

Fig. 5. Top view flow photos at steady or statistical state taken at $y = 0.5$ for $Ra = 2000$ and Re (a) 5.0, (b) 4.0 and (c) 3.0.

flows, revealed from the instantaneous temperature measurement, indicated that in the region dominated by the regular longitudinal rolls the flow is steady, while the flow is time periodic in the regular transverse vortex flow. These features are illustrated in Figs. 6 and 7. The results in Fig. 6 for a pure transverse vortex flow for $Re = 4$ and $Ra = 4000$ show that the entire flow oscillates at the same frequency ($t_p = 5.6$ s) and amplitude in the duct core where the fully developed transverse rolls prevail. In the duct entry where the transverse rolls are in developing stage and in the side wall region where the viscous effects are strong, weaker flow oscillation is noted. It is of interest to notice that even in the region slightly upstream of the test section the flow oscillates weakly at the same frequency as that in the test section. This is due to the presence of the returning flow in that upstream unheated region associated with the main forced flow blocked by the transverse rolls ahead of it. According to the present data, the oscillation frequency can be correlated as

$$F = 0.45Re + 6.70 \times 10^{-4}Re^3 \qquad (4)$$

Meanwhile, the convection speed of the transverse rolls W_r can be estimated from the relation

$$W_r = 1.3W_m \qquad (5)$$

which is the same as that in our earlier study for a lower aspect ratio duct [20]. Additional thermocouple data given in Fig. 7 for a mixed vortex flow with $Re = 5$ and $Ra = 2500$ further show that in the juncture between the longitudinal and transverse rolls the flow is in an intensive irregular oscillation. Moreover, away from the vortex flow in the duct entry the flow is steady.

3.3. Formation of vortex flow patterns

It is important in the fundamental study of heat transfer and fluid dynamics to unveil the processes through which the vortex structures discussed above are formed under the action of the buoyancy. In the study of the vortex flow formation the experiment is started by setting the Reynolds number at 20.0 and the Rayleigh number at the value for the case to be investigated so that the buoyancy-to-inertia ratio is rather low for a sufficient period of time. Thus, the initial flow ($t < 0$) established in the duct is forced convection dominated. Then, at time $t = 0$ the Reynolds number of the flow is lowered quickly to the level for the specific case to be examined and maintained at this level thereafter for $t > 0$. Note that due to the flow inertia, normally it takes about 10–20 s for the Reynolds number to be reduced to the required level.

Firstly, the formation of the vortex flow comprising of steady longitudinal rolls near the duct sides and nonperiodic traversing transverse waves in the duct core is illustrated in Fig. 8 by showing the top view flow photos at selected time instants following the reduction of Re from 20.0 to 4.0 for $Ra = 1750$. The result in Fig. 8(a) indicates that the initial flow at $t = 0$ is nearly unidirectional with the presence of relatively
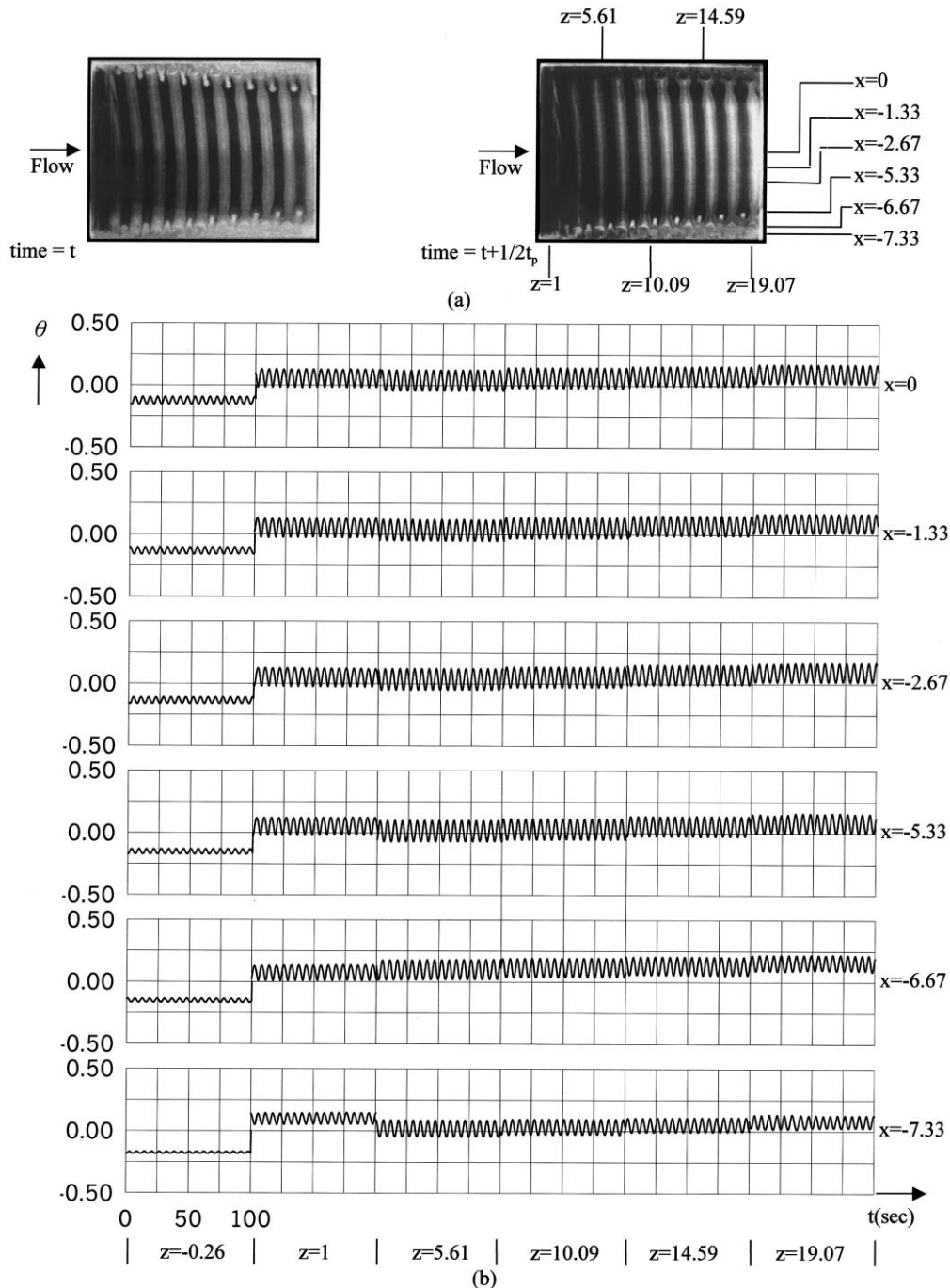

Fig. 6. Temporal structure of vortex flow from (a) top view and (b) time records of air temperature at selected locations on the plane $y = 1/2$ for $Re = 4$ and $Ra = 4000$ ($t_p = 5.6$ s).

weak longitudinal rolls adjacent to the duct sides. Later at $t = 14$ s new longitudinal rolls form adjacent to the existing ones. As time proceeds, additional longitudinal rolls are generated (Fig. 8(c)–(h)). The newly generated rolls are unstable in the beginning (Fig. 8(c)–(f)). However, they gradually stabilize (Fig. 8(g)). It is of interest to note that in almost the entire transient stage nonperiodic traversing transverse waves appear in the region outside the longitudinal rolls, as evident from Fig. 8(b)–(h). The vortex flow
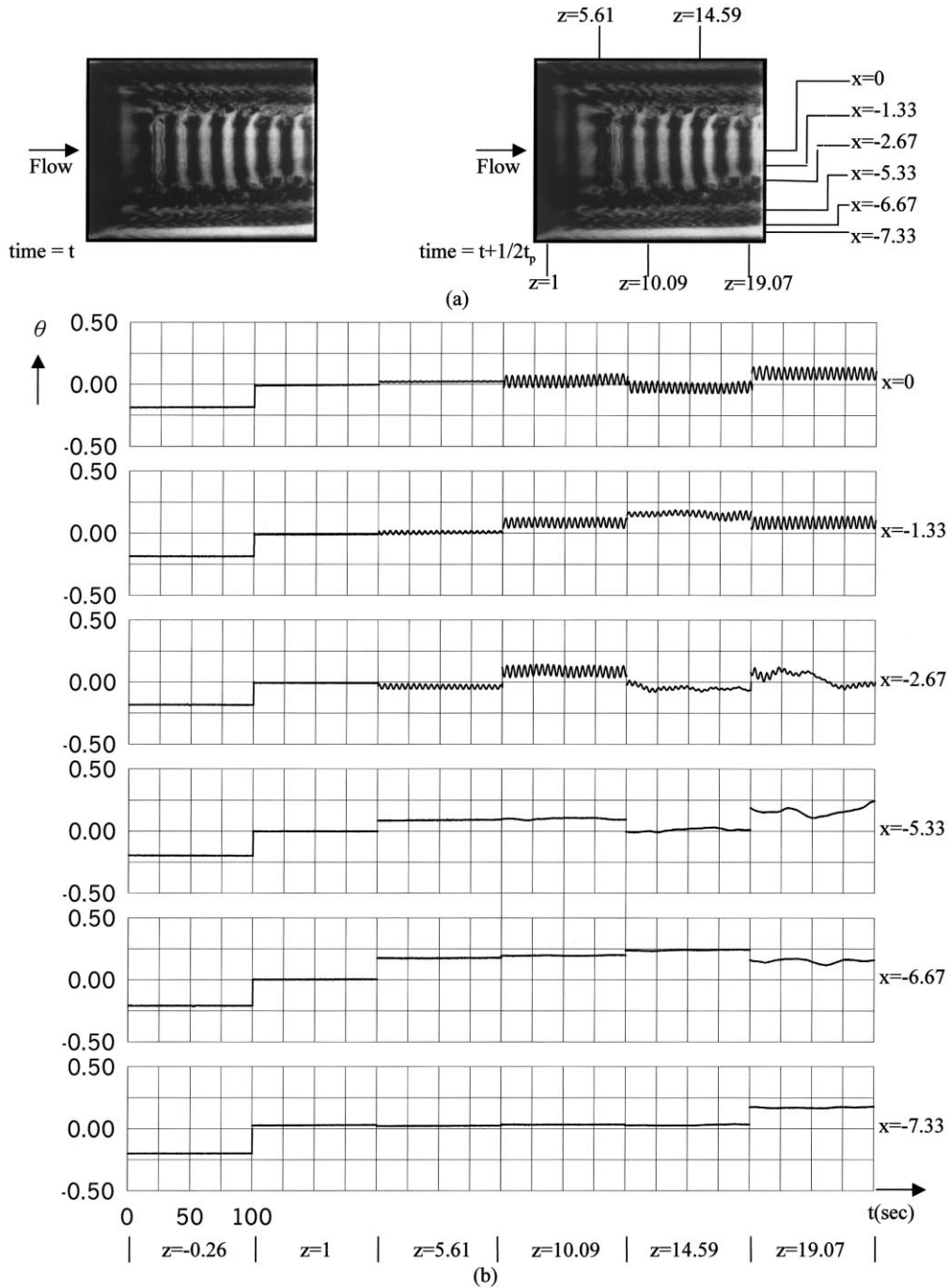

Fig. 7. Temporal structure of vortex flow from (a) top view and (b) time records of air temperature at selected locations on the plane $y = 1/2$ for $Re = 5$ and $Ra = 2500$ ($t_p = 4.6$ s).

pattern in the form of steady longitudinal rolls and traversing waves is thus formed. Note that due to the interaction between the rolls and waves, the longitudinal rolls at largest distance from the duct sides are unstable to some degree (Fig. 8(e)–(h)). At the higher Ra of 2000 for $Re = 5.0$ the traversing waves, however, disappear for $t > 700$ s and a stable longitudinal vortex flow prevails in the duct. Moreover, for cases with $Ra \leq 1650$ at $Re = 4.0$ and 5.0 and for $Ra \leq 1500$ at $Re = 3.0$ traversing transverse waves only appear during the early transient stage and stable longitudinal rolls exist at steady state in the duct.

Next, the formation of the time periodic moving transverse vortex flow and the mixed longitudinal/transverse vortex flow is found to resemble that in our previous study for a lower aspect ratio duct ($A = 12$) [22].

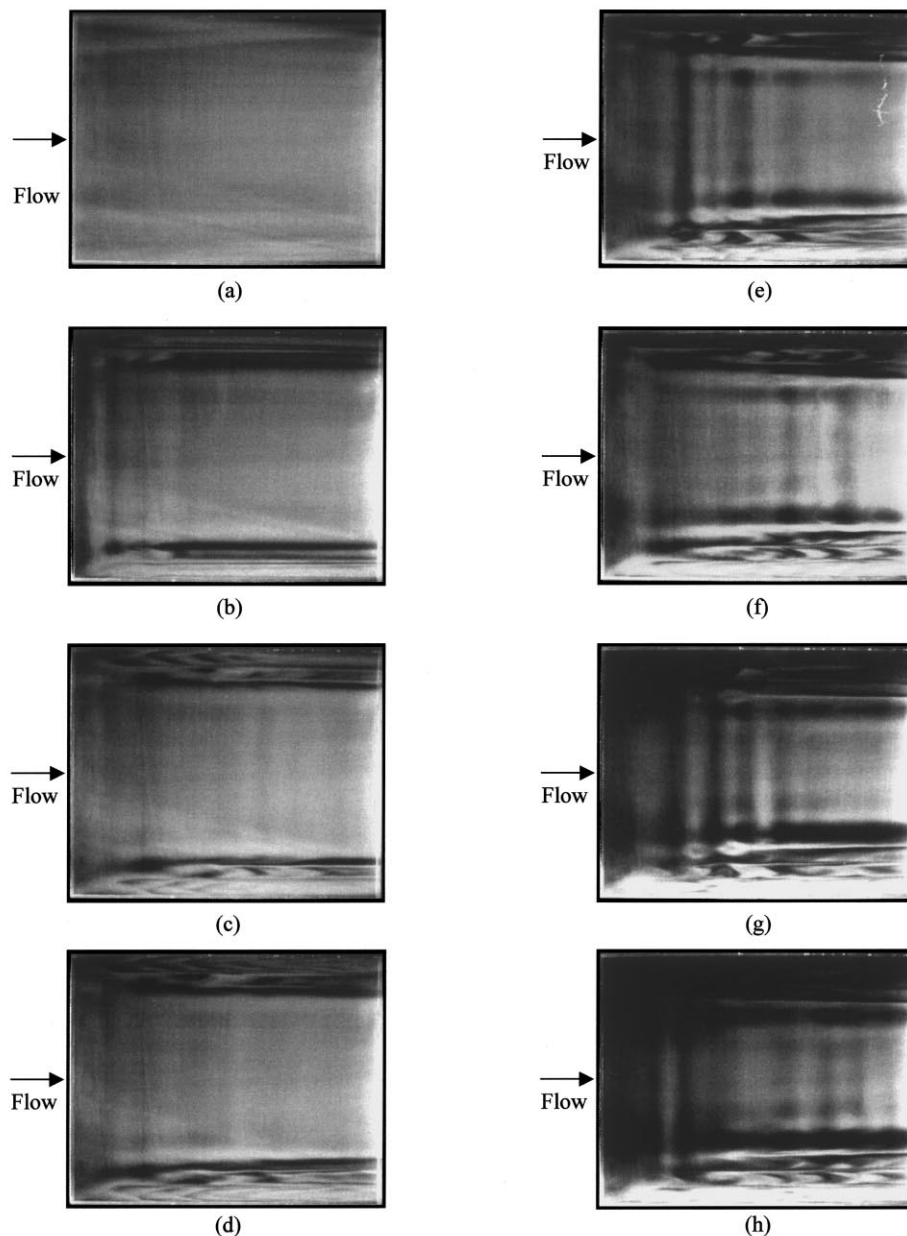Finally, the mixed longitudinal and transverse vortex

Fig. 8. Top view flow photos showing the formation of nonperiodic traversing transverse waves and longitudinal rolls by lowering Re from 20.0 to 4.0 in 12 s for $Ra = 1750$ at time t (a) 0 s, (b) 14 s, (c) 40 s, (d) 81 s, (e) 216 s, (f) 378 s, (g) 2706 s and (h) 4088 s.

flow containing irregular cells prevailed at lower buoyancy than that for the transverse vortex flow is formed through a series of complicate processes shown in Fig. 9 for the case with *Re* reduced from 20.0 to 3.0 at *Ra* = 2000. The results manifest that immediately after the Reynolds number is lowered, a transverse roll is generated at the duct inlet and meanwhile, longitudinal rolls are induced near the duct sides (Fig. 9(b)). However, at this low buoyancy the transverse rolls repeatedly generated at the inlet are weak and only exist in the duct core outside the longitudinal rolls (Fig. 9(c)).

Besides, these downstream moving transverse rolls are somewhat deformed at later time and become knotted (Fig. 9(c)–(e)). Moreover, the knots grow with time and in the adjacent transverse rolls they may contact with each other to form cellular vortex flow in the duct core (Fig. 9(f) and (g)). At this stage the longitudinal rolls near the duct sides are also highly deformed despite of their continuing growth. In addition, we note that the transverse rolls generated at the duct inlet become rather weak. In fact, they consist of a series of traversing transverse waves. These waves
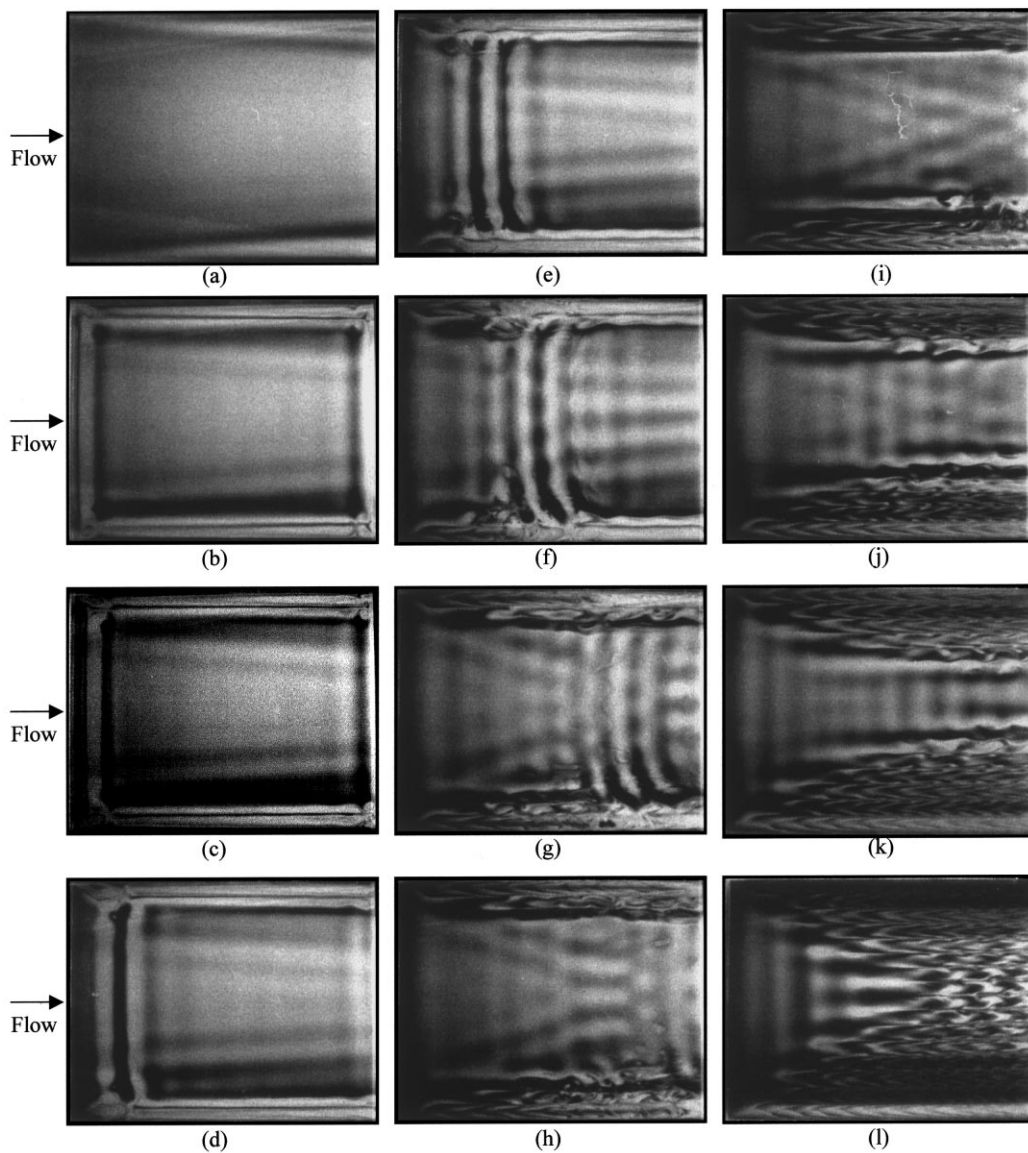

Fig. 9. Top view flow photos showing the formation of mixed longitudinal and transverse rolls and downstream irregular cells by lowering *Re* from 20 to 3 in 6 s at *Ra* = 2000 and *t* (a) 0 s, (b) 11 s, (c) 14 s, (d) 21 s, (e) 30 s, (f) 44 s, (g) 64 s, (h) 81 s, (i) 106 s, (j) 187 s, (k) 276 s, (l) 795 s.

again become knotted and later degenerate into weak, cellular vortex flow. As the weak transverse waves move downstream, the cellular vortex flow ahead of it is pushed slowly out of the duct (Fig. 9(g) and (h)). For a further increase in time additional longitudinal rolls are gradually formed and eventually the downstream portion of the duct is completely filled with longitudinal rolls (Fig. 9(i)–(l)). The irregular vortex cells and transverse waves only exist in the duct core upstream of the longitudinal rolls (Fig. 9(l)). Note that the period of time leading to the mixed vortex flow containing longitudinal and transverse rolls and cells is substantially longer than that for the transverse vortex flow.

4. Concluding remarks

Experimental flow visualization combined with transient temperature measurement have been conducted here to explore the buoyancy driven vortex flow structures in mixed convection of air through a bottom heated horizontal flat duct of a large aspect ratio ($A = 16$). Attention is paid to the flow at a very low Reynolds number ranging from 3.0 to 5.0 and at the Rayleigh number around the critical level for the onset of convection ranging from 1200 to 4000, including the subcritical and supercritical states. Results from the present study reveal that both at subcritical and slightly supercritical Rayleigh numbers steady longitudinal rolls are induced in the duct even at such low Reynolds numbers. In addition to the moving transverse rolls and the mixed longitudinal/transverse rolls which are often observed in the low Reynolds number mixed convection in a horizontal flat duct, some new vortex flow structures are noted in the present study. In particular, we identify two new structures, namely, the stable longitudinal rolls along with the nonperiodic traversing transverse waves and the mixed longitudinal/transverse rolls as well as irregular cells. A flow regime map in terms of Ra vs. Re was given to delineate the induced vortex flow patterns.

The formation processes leading to various vortex flow patterns are rather complicate, including the generation of the longitudinal and transverse rolls and traversing waves, splitting of rolls into cells and the reverse process of integrating cells into rolls, in addition to moving and bending of transverse rolls.

Acknowledgements

References

[1] F.P. Incropera, Convective heat transfer in electronic equipment cooling, J. Heat Transfer 110 (1988) 1097–1111.

[2] W.M. Kays, A.L. London, in: Compact Heat Exchangers, 3rd ed., Mcgraw-Hill, New York, 1984.

[3] G. Evan, R. Grief, A study of traveling wave instabilities in a horizontal channel flow with applications to chemical vapor deposition, Int. J. Heat Mass Transfer 32 (1989) 895–911.

[4] R. Takahashi, Y. Koga, K. Sugawara, Gas flow pattern and mass transfer analysis in a horizontal flow reactor for chemical vapor deposition, J. Electrochem. Soc. 119 (1972) 1406–1412.

[5] M.L. Hitchman, K.F. Jensen, in: Chemical Vapor Deposition-Principles and Applications, Academic Press, San Diego, 1993 (Chapter 2).

[6] E.L. Koschmieder, in: Bernard Cells and Taylor Vortices, Cambridge University Press, Cambridge, 1993 (Chpapter 5).

[7] Y. Mori, Y. Uchida, Forced Convective Heat Transfer between Horizontal Flat Plates, Int. J. Heat Mass Transfer 9 (1966) 803–817.

[8] M. Akiyama, G.J. Hwang, K.C. Cheng, Experiments on the onset of longitudinal vortices in laminar forced convection between horizontal plates, J. Heat Transfer 93 (1971) 335–341.

[9] S. Ostrach, Y. Kamotani, Heat transfer augmentation in laminar fully developed flow by means of heating from below, J. Heat Transfer 97 (1975) 225–225.

[10] Y. Kamotani, S. Ostrach, Effect of thermal instability on thermally developing channel flow, J. Heat Transfer 98 (1976) 62–66.

[11] G.J. Hwang, C.L. Liu, An experimental study of convective instability in the thermal entrance region of a horizontal parallel-plate channel heated from below, Can. J. Chem. Eng. 54 (1976) 521–525.

[12] Y. Kamotani, S. Ostrach, H. Miao, Convective heat transfer augmentation in thremal entrance regions by means of thermal instability, J. Heat Transfer 101 (1979) 222–226.

[13] J.M. Luijkx, J.K. Platten, On the existence of thermoconvective rolls transverse to a superimposed mean Poiseuille flow, Int. J. Heat Mass Transfer 24 (1981) 1287–1291.

[14] J.K. Platten, J.C. Legros, in: Convective in Liquids, Springer-Verlag, Berlin, 1984 (Chapters 6 and 7).

[15] K.C. Chiu, F. Rosenberger, Mixed convection between horizontal plates — I. Entrance effects, Int. J. Heat Mass Transfer 30 (1987) 1645–1654.

[16] K.C. Chiu, J. Ouazzani, F. Rosenberger, Mixed convection between horizontal plates — II. Fully developed flow, Int. J. Heat Mass Transfer 30 (1987) 1655–1662.

[17] M.T. Ouazzani, J.P. Caltagirone, G. Meyer, A. Mojtabi, Etude numérique et expérimentale de la convection mixte entre deux plans horizontaux á températures différences, Int. J. Heat Mass Transfer 32 (2) (1989) 261–269.

[18] M.T. Ouazzani, J.K. Platten, A. Mojtabi, Etude expérimentale de la convection mixte entre deux plans hori-

zontaux á températures différences — II, Int. J. Heat Mass Transfer 33 (7) (1990) 1417–1427.

[19] M.T. Ouazzani, J.K. Platten, A. Mojtabi, Intermittent patterns in mixed convection, Applied Scientific Research 51 (1993) 677–685.

[20] M.Y. Chang, T.F. Lin, Vortex flow pattern selection and temporal-spatial structures of transverse and mixed vortex rolls in mixed convection of air in a horizontal flat duct, Phys. Rev. E54 (1996) 5146–5160.

[21] C.H. Yu, M.Y. Chang, C.C. Huang, T.F. Lin, Unsteady vortex roll structures in a mixed convective air flow through a horizontal plane channel — a numerical study, Int. J. Heat Mass Transfer 40 (3) (1997) 505–518.

[22] M.Y. Chang, C.H. Yu, T.F. Lin, Flow visualization and numerical simulation of transverse and mixed vortex roll formation in mixed convection of air in a horizontal flat duct, Int. J. Heat Mass Transfer 40 (1996) 1907–1922.

[23] M.Y. Chang, C.H. Yu, T.F. Lin, Changes of longitudinal vortex roll structure in a mixed convective air flow through a horizontal plane channel: an experimental study, Int. J. Heat Mass Transfer 40 (2) (1997) 347–363.

[24] C.H. Yu, M.Y. Chang, T.F. Lin, Structure of moving transverse and mixed rolls in mixed convection of air in a horizontal plane channel, Int. J. Heat Mass Transfer 40 (2) (1997) 333–346.

[25] H.K. Moffat, K.F Jensen, Complex flow phenomena in MOCVD reactors, J. Crystal Growth 77 (1986) 108–119.

[26] H.K. Moffat, K.F. Jensen, Three-dimensional flow effects in silicon CVD in horizontal reactors, J. Electro. Chem. Soc. 135 (1988) 459–471.

[27] D.G. Osbrone, F.P. Incropera, Laminar, mixed convection heat transfer for flow between horizontal parallel plates with asymmetric heating, Int. J. Heat Mass Transfer 28 (1985) 207–217.

[28] D.G. Osbrone, F.P. Incropera, Experimental study of mixed convection heat transfer for transitional and turbulent flow between horizontal, parallel plates, Int. J. Heat Mass Transfer 28 (1985) 1337–1344.

[29] F.P. Incropera, A.L. Knox, J.R. Maughan, Mixed-convection flow and heat transfer in the entry region of a horizontal rectangular ducts, J. Heat Transfer 109 (1987) 434–439.

[30] J.R. Maughan, F.P. Incropera, Experiments on mixed convection heat transfer for airflow in a horizontal and inclined channel, Int. J. Heat Mass Transfer 30 (1987) 1307–1318.

[31] R.S. Fligliola, D.E. Beasley, in: Theory and Design for Mechanical Measurements, Wiley, New York, 1995 (Chapter 10).

[32] R.K. Shah, A.L. London, in: Laminar Flow Forced Convective in Ducts, Academic Press, New York, 1987, pp. 196–198.

[33] S.J. Kline, F.A. McClintock, Describing uncertainties in single-sample experiments, Mechanical Engineering 75 (1953) 3–12.